A quadrilateral 2-D finite element based on mixed interpolation of tensorial components

Eduardo N. Dvorkin and Sara I. Vassolo*
Instituto de Materiales y Estructuras, Facultad de Ingeniería, Universidad de Buenos Aires, 1128 Buenos Aires, Argentina
(Received May 1988; revised February 1989)

ABSTRACT

A quadrilateral 2-D finite element for linear and non-linear analysis of solids is presented. The element is based on the technique of mixed interpolation of tensorial components. It is shown that the new element is reliable and efficient, being apt, therefore, to be used in routine engineering applications.

INTRODUCTION

For many years researchers have investigated variational formulations for solid mechanics and the associated finite element techniques. Washizu[1] and Pian and Tong[2] have pioneered in this field and presented a complete classification of the different finite element methods for solid mechanics. Even though most of these methods have rights to claim some particular advantage over the others, the displacement based method has become the most widely used for linear and non-linear analysis of solids and structures. Almost all of the available general purpose finite element codes use mainly displacement based elements.

However, it has been recognized that for some type of problems, the displacement based method provides poor results. Examples are incompressible elasticity and thin plate/shell structures.

Much research effort has been lately directed towards the development of finite elements that while overcoming the drawbacks of the displacement based elements for specific problems, can be used together with them in general purpose finite element codes, providing reliable results. Among many examples we can refer to the hybrid elements developed by Pian and co-workers[2–4]; to the mixed elements developed for incompressible elasticity by Bercovier *et al.*[5] and by Sussman and Bathe[6]; and to the elements based on mixed interpolation of tensorial components developed for the analysis of plate and shell structures by Bathe and Dvorkin[7–9].

In the analysis of 2-D solids the displacement based quadrilateral element also provides poor results. With 4-node element being very desirable for engineering practice, it is an attractive idea to improve their performance by using an alternative formulation[10]. In a previous work Bathe and Dvorkin[9] stated their requirements for reliable shell elements; in the case of 2-D continuum elements those requirements can be recast as:

1. The theoretical formulation of the element must be strongly continuum mechanics based with assumptions in the finite element discretization that are mechanistically clear and well founded for linear and non-linear analysis. The formulation must not incorporate numerically adjusted factors.
2. The element must not contain any spurious zero energy mode.
3. The element must satisfy Irons' patch test[11].
4. The predictive capability of the element must be high and relatively insensitive to element distortions and to changes in material properties (e.g. in the case of an elastic material the Poisson ratio approaching its limit value of 0.5 must not excessively deteriorate the element performance).

In this paper, we present a 4-node element based on the method of mixed interpolation of tensorial components[7–9], that overcomes many of the drawbacks of the standard displacement based quadrilateral element and satisfies, as closely as possible, the reliability criteria we stated above.

Our new quadrilateral element has eight 'exterior degrees of freedom' (two displacements per node). Although it looks like a very tempting goal to satisfy the patch test and also obtain high insensitivity to element distortions (conditions 3 and 4), MacNeal[12] demonstrated that in the case of quadrilateral elements, those two conditions are competitive and there are limits to what can be achieved regardless of the 'interior formulation' of the element.

Taking into account that it is imperative that we assure convergence under any circumstance (even if for some cases the convergence may be slow), in the balance between satisfaction of the patch test and element insensitivity to distortions we must opt for strict satisfaction of the patch test.

* Instituto Nacional de Tecnología Industrial, Buenos Aires, Argentina.

0264-4401/89/030217-08$2.00

THE NEW ELEMENT

To construct our new quadrilateral 2-D finite element based on mixed interpolation of tensorial components we used our accumulated insight into the behaviour of elements to satisfy the previously stated element requirements as closely as possible. As a basic tool to test our developments we used the patch test, after which we measured the order of convergence of the elements under examination by solving some well-established problems.

Geometrically linear analysis

When formulating our element using the method of mixed interpolation of tensorial components we need to adopt a displacement interpolation, a strain interpolation and tie both interpolations together.

To interpolate the displacement field inside the element we use the interpolation functions of a 5-node isoparametric element (see *Figure 1a*).

In the natural coordinate system of an element we can write the strain tensor using covariant components ($\tilde{\varepsilon}_{ij}$) and contravariant base vectors ($\mathbf{g}^i$)[13],

$$\varepsilon=\tilde{\varepsilon}_{rr}\mathbf{g}^r\mathbf{g}^r+\tilde{\varepsilon}_{ss}\mathbf{g}^s\mathbf{g}^s+\tilde{\varepsilon}_{rs}(\mathbf{g}^r\mathbf{g}^s+\mathbf{g}^s\mathbf{g}^r)+\tilde{\varepsilon}_{tt}\mathbf{g}^t\mathbf{g}^t \quad (1)$$

where $\tilde{\varepsilon}_{tt}=0$ for plane strain problems.

We define $\hat{\mathbf{g}}_i=\mathbf{g}_i|_{r=s=0}$ (element centre) and $\hat{\mathbf{g}}^i=\mathbf{g}^i|_{r=s=0}$.

At any point inside the element we can also write,

$$\varepsilon=\hat{\varepsilon}_{rr}\hat{\mathbf{g}}^r\hat{\mathbf{g}}^r+\hat{\varepsilon}_{ss}\hat{\mathbf{g}}^s\hat{\mathbf{g}}^s+\hat{\varepsilon}_{rs}(\hat{\mathbf{g}}^r\hat{\mathbf{g}}^s+\hat{\mathbf{g}}^s\hat{\mathbf{g}}^r)+\hat{\varepsilon}_{tt}\hat{\mathbf{g}}^t\hat{\mathbf{g}}^t \quad (2)$$

where $\hat{\varepsilon}_{ij}=\tilde{\varepsilon}_{lm}(\hat{\mathbf{g}}_i\cdot\mathbf{g}^l)(\mathbf{g}^m\cdot\hat{\mathbf{g}}_j)$.

To interpolate the strain field inside the element we use the following interpolation functions,

$$\hat{\varepsilon}_{rr}=\hat{\varepsilon}_{rr}|_{\mathrm{O}}^{\mathrm{DI}}+\frac{\sqrt{3}}{2}(\hat{\varepsilon}_{rr}|_{\mathrm{D}}^{\mathrm{DI}}-\hat{\varepsilon}_{rr}|_{\mathrm{B}}^{\mathrm{DI}})\frac{|J_0|}{|J|}r+\frac{\sqrt{3}}{2}(\hat{\varepsilon}_{rr}|_{\mathrm{A}}^{\mathrm{DI}}-\hat{\varepsilon}_{rr}|_{\mathrm{C}}^{\mathrm{DI}})\frac{|J_0|}{|J|}s \quad (3a)$$

$$\hat{\varepsilon}_{ss}=\hat{\varepsilon}_{ss}|_{\mathrm{O}}^{\mathrm{DI}}+\frac{\sqrt{3}}{2}(\hat{\varepsilon}_{ss}|_{\mathrm{D}}^{\mathrm{DI}}-\hat{\varepsilon}_{ss}|_{\mathrm{B}}^{\mathrm{DI}})\frac{|J_0|}{|J|}r+\frac{\sqrt{3}}{2}(\hat{\varepsilon}_{ss}|_{\mathrm{A}}^{\mathrm{DI}}-\hat{\varepsilon}_{ss}|_{\mathrm{C}}^{\mathrm{DI}})\frac{|J_0|}{|J|}s \quad (3b)$$

$$\hat{\varepsilon}_{rs}=\hat{\varepsilon}_{rs}|_{\mathrm{O}}^{\mathrm{DI}} \quad (3c)$$

For axisymmetric analysis $\hat{\varepsilon}_{tt}=\hat{\varepsilon}_{tt}|^{\mathrm{DI}}$.

In the above, $\hat{\varepsilon}_{ij}|^{\mathrm{DI}}_{\mathrm{A,B,C,D,O}}$ are the tensorial strain components at points A, B, C, D and O (see *Figure 1b*) directly evaluated from the *D*isplacement *I*nterpolation; $|J_0|$ is the element Jacobian at point O ($r=0$, $s=0$); $|J|$ is the element Jacobian at point (r, s).

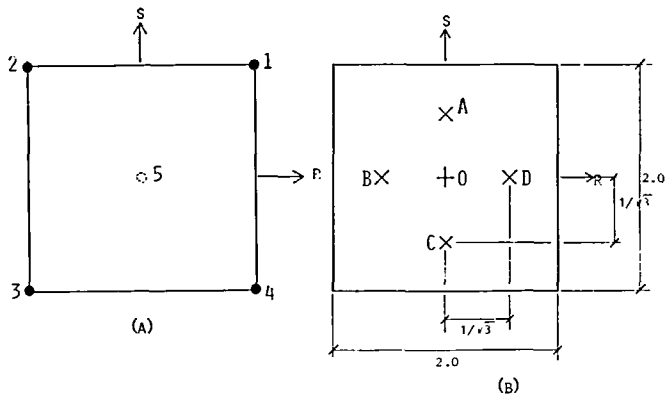

Figure 1 Interpolations used. (a) Nodes used for displacements interpolation. (b) Sample points used for strain interpolation

The adopted strain interpolation:

(1) does not present spurious zero energy modes;
(2) satisfies Irons' patch test (see Appendix I);
(3) can exactly represent, in rectangular elements, a state of plane stress bending (see the numerical tests). This represents an important improvement over the displacement based quadrilateral element.

The two displacements corresponding to node 5 in *Figure 1a* are condensed, as shown in Appendix II, at the element level; therefore the resulting element has only eight degrees of freedom.

Geometrically non-linear analysis

The geometrically non-linear formulation can be developed using either the total Lagrangian formulation[14] or the updated Lagrangian formulation[14]; in this paper we present the first one.

We use the second Piola–Kirchhoff stress tensor[14] as a stress measure and the Green–Lagrange strain tensor[13,14] as a strain measure.

For any instant (load level) t, we refer the strains to the reference configuration at $t=0$, and using (3), the Green–Lagrange strain components are interpolated as,

$${}^t_0\hat{\varepsilon}_{rr}={}^t_0\hat{\varepsilon}_{rr}|_{\mathrm{O}}^{\mathrm{DI}}+\frac{\sqrt{3}}{2}({}^t_0\hat{\varepsilon}_{rr}|_{\mathrm{D}}^{\mathrm{DI}}-{}^t_0\hat{\varepsilon}_{rr}|_{\mathrm{B}}^{\mathrm{DI}})\frac{{}^0|J_0|}{{}^0|J|}r+\frac{\sqrt{3}}{2}({}^t_0\hat{\varepsilon}_{rr}|_{\mathrm{A}}^{\mathrm{DI}}-{}^t_0\hat{\varepsilon}_{rr}|_{\mathrm{C}}^{\mathrm{DI}})\frac{{}^0|J_0|}{{}^0|J|}s \quad (4a)$$

$$ {}_0^t\hat{\varepsilon}_{ss} = {}_0^t\hat{\varepsilon}_{ss}\big|_O^{DI} + \frac{\sqrt{3}}{2}\left({}_0^t\hat{\varepsilon}_{ss}\big|_D^{DI} - {}_0^t\hat{\varepsilon}_{ss}\big|_B^{DI}\right)\frac{{}^0|J_0|}{{}^0|J|}\,r + $$

$$ \frac{\sqrt{3}}{2}\left({}_0^t\hat{\varepsilon}_{ss}\big|_A^{DI} - {}_0^t\hat{\varepsilon}_{ss}\big|_C^{DI}\right)\frac{{}^0|J_0|}{{}^0|J|}\,s \qquad (4b) $$

$$ {}_0^t\hat{\varepsilon}_{rs} = {}_0^t\hat{\varepsilon}_{rs}\big|_O^{DI} \qquad (4c) $$

For axisymmetric analysis ${}_0^t\hat{\varepsilon}_{tt} = {}_0^t\hat{\varepsilon}_{tt}\big|^{DI}$.

The ${}^0|J_0|$ and ${}^0|J|$ are the element Jacobians at (0, 0) and (r, s) evaluated at the reference configuration ($t=0$).

Being ${}_0\hat{\varepsilon}_{ij} = {}^{t+\Delta t}_0\hat{\varepsilon}_{ij} - {}_0^t\hat{\varepsilon}_{ij}$ the increments in the Green–Lagrange strains, we can decompose[14],

$$ {}_0\hat{\varepsilon}_{ij} = {}_0\hat{e}_{ij} + {}_0\hat{\eta}_{ij} \qquad (5) $$

where ${}_0\hat{e}_{ij}$ and ${}_0\hat{\eta}_{ij}$ are the linear and non-linear part of the increments respectively, and are also interpolated using (3).

If we refer the incremental analysis to a fixed Cartesian reference system with base vectors $\mathbf{e}_i$, the Cartesian components of the strains and strain increments are,

$$ {}_0^t\varepsilon_{ij} = \mathbf{e}_i \cdot ({}_0^t\hat{\varepsilon}_{lm}\,{}^0\hat{\mathbf{g}}^l\,{}^0\hat{\mathbf{g}}^m)\cdot\mathbf{e}_j \qquad (6a) $$

$$ {}_0e_{ij} = \mathbf{e}_i \cdot ({}_0\hat{e}_{lm}\,{}^0\hat{\mathbf{g}}^l\,{}^0\hat{\mathbf{g}}^m)\cdot\mathbf{e}_j \qquad (6b) $$

$$ {}_0\eta_{ij} = \mathbf{e}_i \cdot ({}_0\hat{\eta}_{lm}\,{}^0\hat{\mathbf{g}}^l\,{}^0\hat{\mathbf{g}}^m)\cdot\mathbf{e}_j \qquad (6c) $$

where ${}^0\hat{\mathbf{g}}^i$ are the contravariant base vectors at (0, 0), measured in the reference configuration.

The finite element matrices and vectors are calculated using the above interpolations as usual[14].

The two displacements corresponding to node 5 in *Figure 1a* are condensed, as shown in Appendix II, at the element level; therefore the resulting element has only eight degrees of freedom.

NUMERICAL TESTS

In this section we study the numerical behaviour of the new element in an organized way, achieving the following objectives:

(1) We show that the element converges, that is to say[15] that it is stable and consistent.
(2) We examine the solution it provides to some linear problems in order to gain insight into the element performance by comparing its behaviour against the behaviour of other elements.
(3) We examine its response in non-linear analysis.

The numerical solutions we present were all obtained using 2×2 Gauss integration.

In what follows our new element is referred to as QMITC and the displacement based 4-N element as STD-4N.

Convergence check

In order to test the stability of our element we analyse some 'one element cases' using distorted and undistorted elements. The boundary conditions are the minimum necessary to suppress the three physical rigid body modes. No spurious zero energy modes are ever present.

The above is equivalent to examining the eigenvalues of the stiffness matrix corresponding to a free element[16].

In order to test the consistency of the formulation, the patch test needs to be performed. The mesh shown in *Figure 2* is used with the minimum number of boundary conditions needed to suppress the three physical rigid body modes. For all the load cases shown in *Figure 2* the displacements and stresses

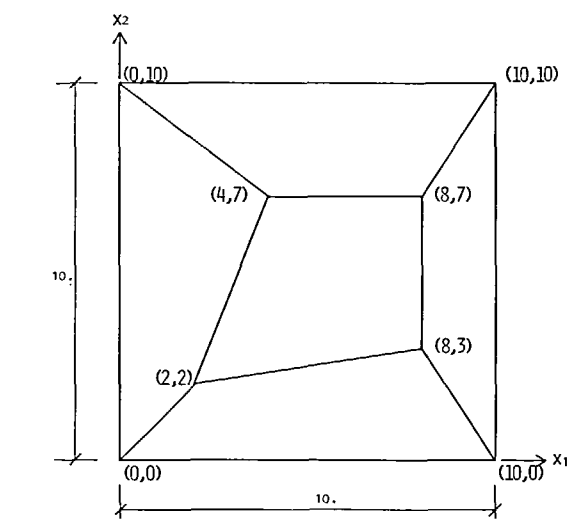

(A) PATCH OF ELEMENTS CONSIDERED

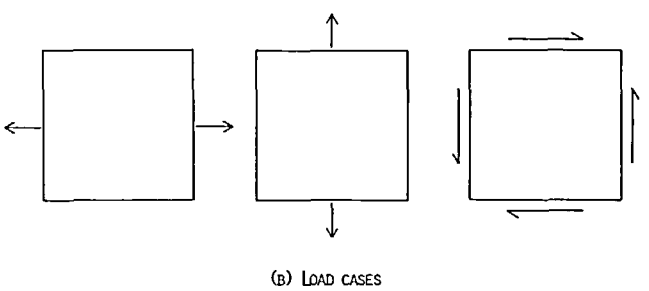

(B) LOAD CASES

Figure 2 Patch tests. (a) Patch of elements considered. (b) Load cases

predicted by the model are identical to the analytical solution.

This numerical results confirm our predictions in Appendix I.

Linear problems

Plane stress rectangular elements under constant bending. In *Figure 3a* we show one rectangular QMITC element under constant bending, the displacement and stresses predicted by the element are identical to the analytical solution.

In *Figure 3b* we compare the results of the QMITC element against the results of the STD-4N, for a mesh of rectangular elements under constant bending. While the aspect ratio deteriorates the behaviour of the standard element, it does not affect the results of the new element.

Plane stress rectangular elements under linear varying bending. In *Figure 4* we compare the results of the QMITC and STD-4N elements for a mesh of rectangular elements under linear varying bending. The convergence for the new element is much faster than for the standard one.

Plane stress distorted elements under constant bending. Although for the mesh shown in *Figure 5a*,

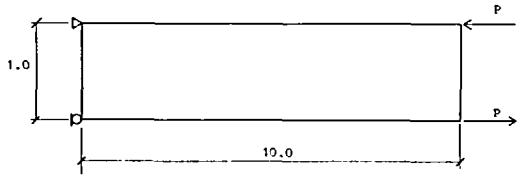

E = 1000.
ν = 0.3
thickness = 0.1

(A)

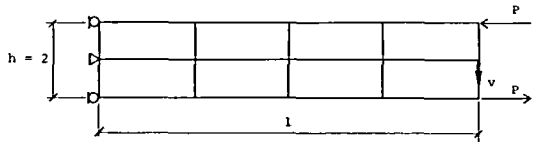

E = 1000.
ν = 0.0
thickness = 1.0

l/h	$v^{FEM}/v^{ANALYT.}$	
	QMITC	STD-4N
5.	1.00	0.56
10.	1.00	0.24
50.	1.00	0.013
100.	1.00	0.0032

(B)

Figure 3 Plane stress rectangular elements under constant bending. (a) One element case. (b) Mesh of rectangular elements

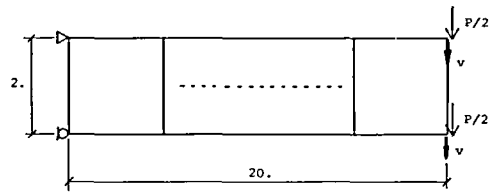

E = 1000.
ν = 0.0
thickness = 1.0

N	$v^{FEM}/v^{ANALYT.}$	
	QMITC	STD-4N
1	0.76	0.02
2	0.94	0.07
3	0.98	0.16
4	0.99	0.24
5	1.00	0.34

Figure 4 Plane stress rectangular elements under linear varying bending

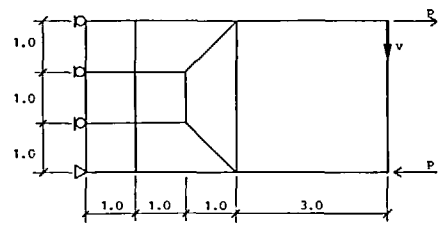

E = 1.0
ν = 0.25
thickness = 1.0

	$v^{FEM}/v^{ANALYT.}$
QMITC	0.948
STD-4N	0.829

(A)

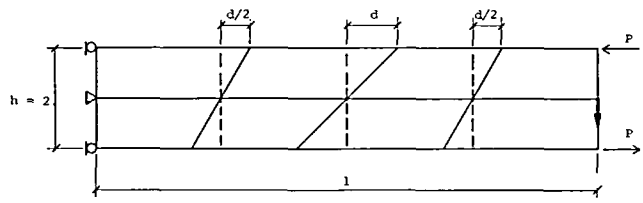

E = 1000.
ν = 0.0
thickness = 1.0

l/h	$v^{FEM}/v^{ANALYT.}$			
	d = 1.0		d = 2.0	
	QMITC	STD-4N	QMITC	STD-4N
5	0.852	0.403	0.631	0.250
10	0.824	0.161	0.615	0.097

(B)

Figure 5 Plane stress distorted elements under constant bending. (a) Distorted mesh I. (b) Distorted mesh II

which was also used by Pian and Sumihara[4], there is a fairly good agreement between the results provided by the QMITC element and the analytical results; the results obtained with the mesh in *Figure 5b* are not so close to the analytical ones, but are always better than those provided by the STD-4N element.

As demonstrated by MacNeal[12], the results of quadrilateral elements deteriorate when trapezoidal elements are used.

It is important to point out, however, that Pian and Sumihara[4] presented a hybrid element with four incompatible modes and stress interpolation in the natural coordinate system, which seems to be more insensitive to element distortions than the QMITC.

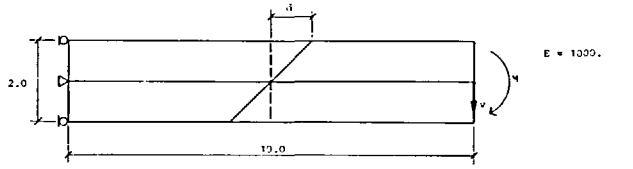

ν	$v^{FEM}/v^{ANALYT.}$					
	d = 0.0		d = 0.5		d = 1.0	
	QMITC	STD-4N	QMITC	STD-4N	QMITC	STD-4N
0.000	1.00	0.24	0.77	0.13	0.54	0.13
0.100	0.99	0.26	0.77	0.20	0.54	0.14
0.200	0.96	0.27	0.75	0.21	0.54	0.14
0.300	0.91	0.28	0.72	0.21	0.52	0.14
0.400	0.84	0.27	0.67	0.19	0.49	0.13
0.450	0.80	0.25	0.63	0.16	0.47	0.12
0.490	0.76	0.10	0.61	0.06	0.46	0.08
0.499	0.75	0.02	0.60	0.02	0.45	0.03

(a)

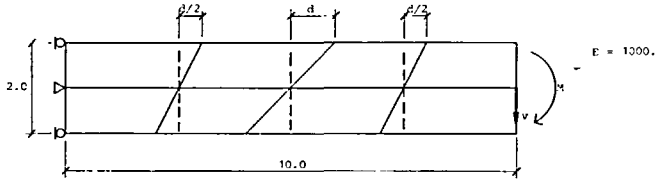

ν	$v^{FEM}/v^{ANALYT.}$			
	d = 0.0		d = 1.0	
	QMITC	STD-4N	QMITC	STD-4N
0.000	1.00	0.56	0.86	0.41
0.200	0.96	0.58	0.85	0.41
0.400	0.85	0.50	0.76	0.32
0.450	0.80	0.41	0.73	0.25
0.480	0.78	0.27	0.70	0.16
0.490	0.77	0.17	0.70	0.12
0.499	0.76	0.02	0.69	0.03

(b)

Figure 6 Plane strain elements under constant bending. (a) Mesh I. (b) Mesh II

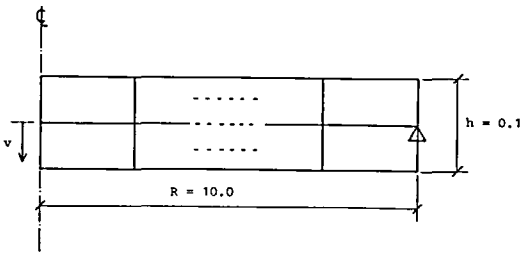

N	$v^{FEM}/v^{ANALYT.}$	
	QMITC	STD-4N
1	0.616	0.0013
2	0.898	0.0078
3	0.954	0.0206
4	0.974	0.0400
5	0.984	0.0652

Figure 7 Simply supported circular plate under concentrated load

Plane strain elements under constant bending. In *Figure 6* we compare the results provided by the QMITC element against the results of the STD-4N element, for two different meshes, both in plane strain and under constant bending.

The QMITC results are much better than the standard element results and more insensitive to an increasing Poisson ratio.

A similar test was used by Taylor *et al.*[16] to investigate the effect on the element performance of an increasing Poisson ratio combined with elements distortions.

Simply supported circular plate under a concentrated central load. In *Figure 7* we show a simply supported circular plate ($R/h = 100$), under a concentrated central load, modelled using axisymmetric elements.

The QMITC results show a fast convergence.

Thermal loads. Usually when analysing problems involving thermal loading, it is more difficult to achieve good finite element results than when analysing problems involving mechanical loading[17].

When using the STD-4N element for thermoelastic problems we interpolate the temperatures with the displacement interpolation functions as it is usually done. When using the QMITC element we interpolate the thermal strains $\varepsilon_{ij}^{TH} = \alpha\theta\delta_{ij}$ using (3) (α is the thermal expansion coefficient, θ is the point temperature and δ_{ij} is the Kronecker delta).

In *Figure 8* we show a rectangular element free to dilatate. When the element is under constant temperature both, the QMITC and the STD-4N,

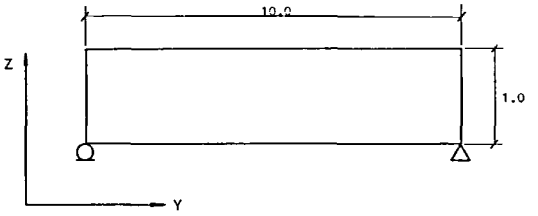

E = 3 E+05
α = 0.1 E-04
ν = 0.2
Plane stress
θ_{ref} = const.

$\theta = a + b\,y + c\,z$

	$\max\left[\frac{\sigma^{REF}_{trial}}{E\,\alpha\,(\theta-\theta_{ref})}\right]$
QMITC	0.0
STD-4N	6.65

Figure 8 Thermal loading

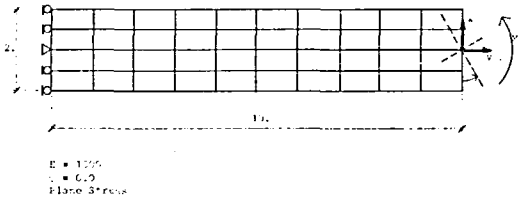

Figure 9 Cantilever with large displacements

provide the exact displacements and the exact stresses ($\sigma_{ij}=0.0$) because both elements satisfy the patch test.

But when we impose a linear temperature distribution of the form $\theta=a+by+cz$, even though the analytical solution is $\sigma_{ij}=0.0$, the STD-4N element predicts big parasitic stresses while the QMITC element provides the exact solution.

Non-linear problem

In *Figure 9* we show a cantilever under constant bending and its analytical results compared against the results provided by the QMITC and STD-4N elements, using the total Lagrangian formulation.

The new element delivers much better results than the standard element, even though we use a coarse mesh, considering that the final tip rotation is of 45 degrees.

CONCLUSIONS

A quadrilateral 2-D finite element, based on the technique of mixed interpolation of tensorial components was presented.

The element does not contain spurious zero energy modes and passes the patch test. In Appendix I a rational method for designing strain interpolations that lead to the satisfaction of the patch test is presented, we hope that this will foster the development of more and more efficient mixed interpolated elements.

The new quadrilateral element satisfies our reliability requirements presented in the Introduction, and although the numerical results show that it is not as insensitive to element distortions as desirable, MacNeal[12] demonstrated that there is a limit in what can be achieved in this regard, with elements presenting only eight 'exterior degrees of freedom'.

We believe that the present element also constitutes a good basis for the future design of the in-layer strain interpolation of new quadrilateral shell elements[7].

ACKNOWLEDGEMENT

This research was carried out in the framework of a joint research agreement between the Instituto de Materiales y Estructuras and the Instituto Nacional de Tecnología Industrial.

REFERENCES

1 Washizu, K. *Variational Methods in Elasticity and Plasticity*, 3rd edn, Pergamon Press, Oxford and New York (1982)
2 Pian, T. H. H. and Tong, P. Basis of finite element methods for solid continua, *Int. J. Num. Meth. Eng.*, **1**, 3–28 (1969)
3 Pian, T. H. H. Variational and finite element methods in structural analysis, *RCA Rev.*, **39**, 648–664 (1978)
4 Pian, T. H. H. and Sumihara, K. Rational approach for assumed stress finite elements, *Int. J. Num. Meth. Eng.*, **20**, 1685–1695 (1984)
5 Bercovier, M., Hasbani, J., Gilon, J. and Bathe, K. J. On a finite element procedure for nonlinear incompressible elasticity, *Hybrid and Mixed Finite Element Methods* (Eds. Atluri *et al.*), John Wiley, Chichester (1983)
6 Sussman, T. and Bathe, K. J. A finite element formulation for nonlinear incompressible elastic and inelastic analysis, *Comp. Struct.*, **26**, 357–409 (1987)
7 Dvorkin, E. N. and Bathe, K. J. A continuum mechanics based four-node shell element for general nonlinear analysis, *Eng. Comp.*, **1**, 77–88 (1984)
8 Bathe, K. J. and Dvorkin, E. N. A four-node plate bending element based on Mindlin/Reissner plate theory and a mixed interpolation, *Int. J. Num. Meth. Eng.*, **21**, 367–385 (1985)

9 Bathe, K. J. and Dvorkin, E. N. A formulation of general shell elements—the use of mixed interpolation of tensorial components, *Int. J. Num. Meth. Eng.*, **22**, 697–722 (1986)
10 Cook, R. D. Improved two-dimensional finite element, *ASCE J. Struct. Div.*, **ST9**, 1851–1863 (1974)
11 Irons, B. M. and Razzaque, A. Experience with the patch test for convergence of finite elements, in *The Mathematical Foundation of the Finite Element Method with Applications to Partial Differential Equations* (Ed. A. K. Aziz), Academic Press, London and New York (1972)
12 MacNeal, R. H. A theorem regarding the locking of tapered four-noded membrane elements, *Int. J. Num. Meth. Eng.*, **24**, 1793–1799 (1987)
13 Green, A. E. and Zerna, W. *Theoretical Elasticity*, 2nd edn, Oxford University Press, Oxford (1968)
14 Bathe, K. J. *Finite Element Procedures in Engineering Analysis*, Prentice-Hall, Englewood Cliffs, NJ (1982)
15 Strang, G. and Fix, G. J. *An Analysis of the Finite Element Method*, Prentice-Hall, Englewood Cliffs, NJ (1973)
16 Taylor, R. L., Simo, J. C., Zienkiewicz, O. C. and Chan, A. C. The patch-test. A condition for assessing FEM convergence, *Int. J. Num. Meth. Eng.*, **22**, 39–62 (1986)
17 Pittr, J. and Hartl, H. Improved stress evaluation under thermal load for simple finite elements, *Int. J. Num. Meth. Eng.*, **15**, 1507–1515 (1980)
18 Przemieniecki, J. S. *Theory of Matrix Structural Analysis*, McGraw-Hill, New York (1968)

APPENDIX I

The patch test

In the numerical study of our element we performed the patch tests shown in *Figure 2*. For each of these tests the patch of elements is subjected to:

- displacement boundary conditions just sufficient to remove all physical rigid body modes;
- externally applied boundary nodal point forces that correspond to constant boundary stress conditions.

The analysis yields the nodal point displacements and the internal element stresses. The patch test is passed if these predicted quantities are identical to the analytical solution.

Therefore, in order to pass the patch test, the strain interpolation of the element needs to satisfy the following two requirements.

First requirement. The strain interpolation must be able to represent for any element geometry a state of constant strain with analytically correct nodal point displacements. By inspection of (3) it is obvious that the strain interpolation we adopted satisfies this first requirement.

Second requirement. For the displacement based quadrilateral element[14]:

$$\mathbf{u}=\mathbf{H}_4\mathbf{U}$$

$$\boldsymbol{\varepsilon}=\mathbf{B}\mathbf{U}$$

where $\mathbf{u}^T=(u_x\ u_y)$ and $\mathbf{U}$ is the vector of nodal displacements.

For this case $\mathbf{B}$ is derived in the standard way[14] and the element satisfies the patch test.

In the patch test situation $\boldsymbol{\sigma}=\boldsymbol{\sigma}^*=$const. and being $\mathbf{t}$ the surface tractions, the Principle of Virtual Work[1,14] states

$$\delta\mathbf{U}^T\left[\int_V \mathbf{B}^T\,dV\right]\boldsymbol{\sigma}^*=\delta\mathbf{U}^T\int_S \mathbf{H}s_4^T\mathbf{t}\,dS \qquad (A1)$$

where $\mathbf{H}s_4$ is $\mathbf{H}_4$ specialized for the element sides.

For the element based on mixed interpolation of tensorial components

$$\mathbf{u}=\mathbf{H}_5\mathbf{U}$$

$$\boldsymbol{\varepsilon}=\hat{\mathbf{B}}\mathbf{U}$$

For this case $\hat{\mathbf{B}}$ is formed using (3).

For the patch test situation,

$$\delta\mathbf{U}^T\left[\int_V \hat{\mathbf{B}}\,dV\right]\boldsymbol{\sigma}^*=\delta\mathbf{U}^T\int_S \mathbf{H}s_5^T\mathbf{t}\,dS \qquad (A2)$$

As $\mathbf{H}s_5=\mathbf{H}s_4$, (A1) and (A2) lead to the second requirement for the satisfaction of the patch test,

$$\int_V \hat{\mathbf{B}}\,dV=\int_V \mathbf{B}\,dV \qquad (A3)$$

The strain interpolations presented in (3), satisfy the above requirement.

APPENDIX II

Element matrices condensation

Linear static analysis. In the QMITC element $\mathbf{U}^T=(\mathbf{U}_e^T\ \mathbf{U}_i^T)$, where $\mathbf{U}_e$ is the vector containing the displacements of nodes 1 to 4 and $\mathbf{U}_i$ contains the displacements of node 5.

Since there are no external loads acting on node 5,

$$\begin{bmatrix}\mathbf{K}_{ee} & \mathbf{K}_{ei}\\ \mathbf{K}_{ie} & \mathbf{K}_{ii}\end{bmatrix}\begin{bmatrix}\mathbf{U}_e\\ \mathbf{U}_i\end{bmatrix}=\begin{bmatrix}\mathbf{P}\\ \mathbf{0}\end{bmatrix} \qquad (B1)$$

From the above,

$$\mathbf{U}_i=-\mathbf{K}_{ii}^{-1}\mathbf{K}_{ie}\mathbf{U}_e \qquad (B2)$$

$$(\mathbf{K}_{ee}-\mathbf{K}_{ei}\mathbf{K}_{ii}^{-1}\mathbf{K}_{ie})\mathbf{U}_e=\mathbf{P} \qquad (B3)$$

Non-linear static analysis. For the j-iteration[14] in the step from the configuration at time (load level) t to $t+\Delta t$

$$\begin{bmatrix}\mathbf{K}_{ee} & \mathbf{K}_{ei}\\ \mathbf{K}_{ie} & \mathbf{K}_{ii}\end{bmatrix}\begin{bmatrix}\Delta\mathbf{U}_e^{(j)}\\ \Delta\mathbf{U}_i^{(j)}\end{bmatrix}=\begin{bmatrix}{}^{t+\Delta t}\mathbf{P}\\ \mathbf{0}\end{bmatrix}-\begin{bmatrix}{}^{t+\Delta t}\mathbf{F}_e^{(j-1)}\\ {}^{t+\Delta t}\mathbf{F}_i^{(j-1)}\end{bmatrix} \qquad (B4)$$

From the above,

$$\Delta \mathbf{U}_i = -\mathbf{K}_{ii}^{-1}({}^{t+\Delta t}\mathbf{F}_i^{(j-1)} + \mathbf{K}_{ie}\Delta \mathbf{U}_e^{(j)}) \quad \text{(B5)}$$

$$(\mathbf{K}_{ee} - \mathbf{K}_{ei}\mathbf{K}_{ii}^{-1}\mathbf{K}_{ie})\Delta \mathbf{U}_e^{(j)} = {}^{t+\Delta t}\mathbf{P} - ({}^{t+\Delta t}\mathbf{F}_e^{(j-1)} - \mathbf{K}_{ei}\mathbf{K}_{ii}^{-1}\,{}^{t+\Delta t}\mathbf{F}_i^{(j-1)}) \quad \text{(B6)}$$

Dynamic analysis. As shown by Przemieniecki[18], the condensed mass matrix is given

$$\mathbf{M}_c = \mathbf{A}_c^{\mathrm{T}}\mathbf{M}\mathbf{A}_c \quad \text{(B7)}$$

where

$$\mathbf{A}_c = \begin{bmatrix} \mathbf{I} \\ -\mathbf{K}_{ii}^{-1}\mathbf{K}_{ie} \end{bmatrix} \quad \text{(B8)}$$

In the above, $\mathbf{M}_c$ is the condensed mass matrix, and $\mathbf{M}$ is the mass matrix before condensation.